

Flight Force Measurements for a Micromechanical Flying Insect

R. J. Wood R.S. Fearing

Department of EECS, University of California, Berkeley, CA 94720
{rjwood, ronf}@robotics.eecs.berkeley.edu

Abstract

Key to the success of the micromechanical flying insect project is developing sensors for flight force measurement. At the lowest level of MFI control is the wing control system which will rely on wing and thorax mounted force sensors. These sensors will have the dual function of stroke by stroke force characterization and system identification as well as use in feedback control for all levels. There are two methods for force sensing on a flying robotic insect, measurements directly on the thorax, and body force measurement with a tradeoff in design between sensor bandwidth and sensitivity.

1.0 Introduction

The Micromechanical Flying Insect (MFI) project [6], [13] aims to create a robotic insect, with a wingspan of 25mm, capable of sustained autonomous flight. Yan, et al suggested in [13] that force feedback would be both feasible and necessary for control in a micromechanical flying insect. It has been shown by Nalbach in [9] that insects such as *Calliphora* use sophisticated means to measure forces and torques for complicated guidance systems. The MFI will use a hierarchical control/sensor system, broken into the higher level of mission control down to individual wing control. The MFI is very biomimetic in nature, and the methods of force/torque sensing which are used are no exception. For autonomous strain sensing, the MFI will use a system very similar to insect campaniform sensilla (see [3]).

Traditionally, measuring forces on a flying insect is performed by fixing the insect to a cantilever and optically measuring its position, or by measuring air flow vectors using particle image velocimetry (PIV) [7]. These methods will work with the MFI, however there are two reasons for avoiding it. First, it is desired to measure the forces autonomously during flight, where optical force reading would not be possible, and PIV would be difficult. Second, the nature of the forces generated by the MFI make it only necessary to measure certain torques, as will be discussed in section 2. Thus the MFI is best suited for either direct wing force measurement or body force measurement by way of cantilever based strain sensors.

Each method of force sensing described in this paper has associated benefits and difficulties. Measuring the

forces generated by the MFI using off board, or body force sensors, give the benefits high sensitivity, and ease of use. Measuring the forces directly on the wing spar gives the benefit of being useable at the final scale, while increasing difficulty in construction. Finally, placing strain sensors directly on the actuator makes for easier installation, allows system identification, gives the ability to sense position, and can be used to protect the actuator from high strains. The main concern in the design of force sensors for microrobotics is sensitivity and bandwidth along with small size and low mass. What is unique about the MFI is the need for both high sensitivity due to small forces, and high bandwidth due to high wing beat frequency.

The MFI currently uses folding processes described by Shimada in [12]. The goal of obtaining flight force measurements was not only to design high sensitivity, high bandwidth sensors for the MFI, but to integrate them into the current process. This paper describes three methods of measuring the forces generated by autonomous flying robotic insects, and gives preliminary results from tests done on the MFI thorax.

2.0 Forces Acting on the MFI

Most flying insects, such as the blowfly *Calliphora*, have control over three degrees of freedom (DOF) in their wing motion. These three degrees of freedom consist of the wing angle, angle of attack, and out of stroke plane deviation. Of these three, the MFI will use only the two most vital; wing position and angle of attack. These motions are achieved by using piezo-electric actuators, driving a mechanical amplifying thorax structure [13]. The free ends of the actuators are connected to slider crank mechanisms which convert the linear motion of the actuators into a rotation at the base of the fourbar. The thorax output drives a differential mechanism attached to a rigid wing. From the two 1-DOF four-bars, the wing differential can produce wing motions consisting of the desired flapping and rotations. Flapping occurs when the actuators are in phase, and rotation occurs when the two are out of phase. Figure 1 shows the wing transmission system consisting of two actuators, two fourbars, the wing differential, and the wing.

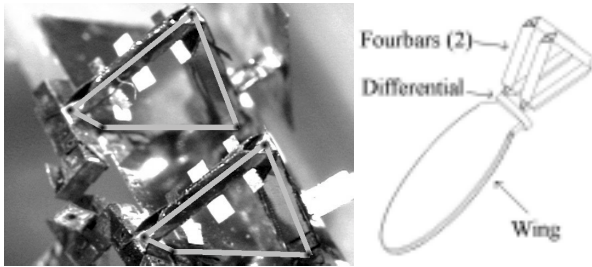


Figure 1: 2 DOF thorax and wing structure

The MFI in free flight has six degrees of freedom (fig. 2), and has the use of two – two DOF wing structures to produce net force/torque vectors in each of these six DOF's. Thus measuring the generated wing forces is a crucial step towards control of the MFI as a whole.

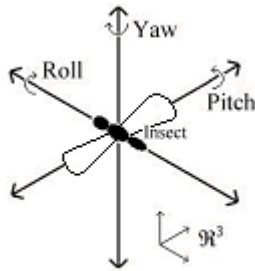


Figure 2: Insect coordinate system

Section 3 describes a method of measuring the forces on the wing by placing sensors on the wing spars, thus the force is measured directly. Section 4 describes a method of measuring the total lift and drag by placing the MFI on a platform which measures the forces generated by the body. Finally, section 5 discusses placing sensors on the actuators as an alternative to placing gages on the wing.

3.0 Direct Force Measurement

Directly measuring the flight forces involves measuring the moments on the wing using strain gages mounted directly in the wing spars. This has been achieved by using semiconductor strain gages bonded directly to each wing spar. This technique has the advantage of being scalable and practical for the final size MFI, and has the downside of difficulty in construction as well as possible interference with overall performance due to its wires. The direct force measurement was achieved in two stages, first at the 5X scale, then at 1.3X scale using similar techniques.

3.1 Wing Spar Sensing

Strain gages are passive structures which change resistance when in compression or tension, thus by

placing the gages across an excitation voltage, it is a simple matter to measure strain. The strain on a material is a unit-less quantity defined by $\epsilon = \Delta l/l$ where l is the length of the material and Δl is the change in length of the material caused by compression or tension. In the case of a rigid body, such as a wing spar, measuring the strain gives the moment directly.

$$M = \frac{EI\epsilon}{z} \quad (1)$$

In the above equation, E is the Modulus of Elasticity, I is the cross sectional moment of inertia, and z is the distance from the gage to the neutral axis. Finally, the force is calculated as a function of the moment on the spar, $M = -F \cdot (l - x)$ where the force acts on the end of the spar of length l . The unit x represents the distance from the fixed end of the cantilever to the point of measurement (the center of the gage).

To begin, a five-times scale wing and four-bar structure was built using the same design and construction techniques as are implemented in the 1.3X scale. Since piezoelectric actuators at this scale would require huge electric fields and produce small amplitudes, voice coil actuators (VCA)s were used to drive the 5X structure. One concern with the spar sensing system is the wiring of the gages. Since the signal must go from the spar, through the thorax to the body, the 5X scale spar was fitted with a circuit board cut from copper using a laser cutting system. The $25\mu\text{m}$ thick copper was affixed to the spar and the gages were placed in gaps in the board directly onto the spar. The strain gages used were 1mm long, $150\mu\text{m}$ wide semiconductors made by Entran, Inc model ESB-20-350. Where the spar connects to the top link of the fourbar mechanism there is a flexible multiconductor cable which winds through the thorax to signal conditioners (Techkor model MEPTS-9000). Wherever possible, the strain gages were setup in a half or full bridge configuration to alleviate thermal drift.

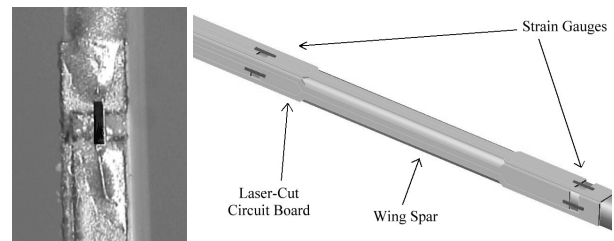


Figure 3: 5X scale wing spar

Testing was done by fixing the base link of the four-bar and driving the side link with a VCA. The VCA is controlled by a real-time ADC/DAC board (Quanser Consulting) connected to a PC, and the position sensed

optically. For this model, optical sensors were fixed to the base of the VCA motion arm, and the nonlinearities were well characterized. The software running the board compiles Simulink models into real-time executables, therefore the test system can be driven closed loop using a simple PD controller to track a position reference.

Initially, a single gage was placed on the wing spar to measure the inertial and aerodynamic forces felt on the tip of the spar. The gage was mounted to a square polystyrene spar and positioned on the four-bar as in figure 3. The position of the gage along the spar is crucial for the sensitivity of the measurements. For a given force, the maximum moment, and thus the maximum strain is measured when the gage is placed as close to the base of the cantilever as possible.

However, during a wing stroke, the greatest forces will not always act on the end of the spar. For this reason another gage was added to the spar to measure the moments at two different positions. Any force distribution along a rigid body is equivalent to a single force and moment acting on one point. Using this assumption, the equivalent force and position vector can be measured. By measuring the moment at two positions this can be resolved from the following:

$$\begin{aligned} M_1 &= F_{eq} (x_1 - x_{eq}) \\ M_2 &= F_{eq} (x_2 - x_{eq}) \end{aligned} \quad (2)$$

Where F_{eq} is the equivalent force at x_{eq} , the center of force. This method was then implemented on two orthogonal faces of the spar, allowing two sensing degrees of freedom. The results for the 5X are discussed in section 3.2.

Since the strain gages are sufficiently small, the same gages were used on the 1.3X scale wing spar. As with the 5X scale, there are two ways of getting the signals off of the 1.3X spar, either the wiring is a part of the base flexure, or the wiring comes off the spar directly. In the case of the wiring being a part of the flexure, this would involve using some type of metalization onto the polyester flexure. This may cause problems, however, since the flexure is subject to large strains which would cause a change in the resistivity of any metal deposited on the surface. This would in essence create a second set of strain gages on the flexure, giving erroneous signals. The alternative, taking the wires off the spar directly also has a number of concerns. First, the wires add a parallel stiffness to the system, lowering the stroke angle and resonant frequency. Second, putting the wires through a large angle at high frequencies results in high fatigue and in wires breaking (which was certainly the case during testing). However, the approach taken, mostly for

convenience sake, was to take the wires off the spar and form them into very compliant springs. This way the strain will be distributed through the spring, and the parallel compliance will not be significant enough to cause any attenuation in stroke amplitude. Table 1 gives the design parameters for direct force measurement at both the 5X and 1.3X scales.

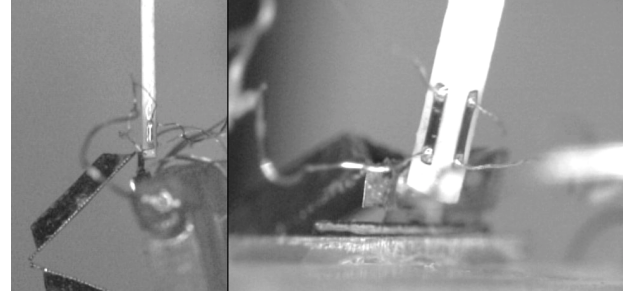


Figure 4: Two-axis strain gage configuration on .5mm square polystyrene spar

Parameter	Description	Value	Units
F_{min}	Sensitivity	1.00E-05	N
E	Young's Modulus (Polystyrene)	3.00E+00	GPa
w_1	Spar Width (5X scale)	1.00E-03	m
w_2	Spar Width (1.3X scale)	5.00E-04	m
l_1	Spar Length (5X scale)	5.00E-02	m
l_2	Spar Length (1.3X scale)	1.00E-02	m
l_w	Wing Length (5X scale)	5.00E-02	m
l_w	Wing Length (1.3X scale)	1.00E-02	m
J_w	Wing Inertia (5X scale)	8.40E-10	kgm ²
J_w	Wing Inertia (1.3X scale)	7.00E-11	kgm ²

Table 1: Wing sensor design parameters

3.2 Spar Sensing Results

The forces measured on the wing spar are on average 90% inertial for Calliphora-like wings with relatively small damping. This ratio is determined by the Q of the thorax.

$$\begin{aligned} \tau_{inertial} &= J_w \omega^2 A \\ \tau_{aero} &= B_w \omega A \\ \frac{\tau_{inertial}}{\tau_{aero}} &= \frac{J_w \omega}{B_w} \equiv Q \end{aligned} \quad (3)$$

Thus the desired signal is small compared to the total signal. To compensate, the wing was set orthogonal to the drag plane, actuated, and the forces measured were assumed to be purely inertial. At the 5X scale, the wings went through a wing stroke of 50° at a frequency of 16Hz. The forces were measured by fixing the wing at a set angle of attack in the stroke plane and actuated to

measure peak-to-peak force. The measured results from experiments at the 5X scale are shown in figure 5.

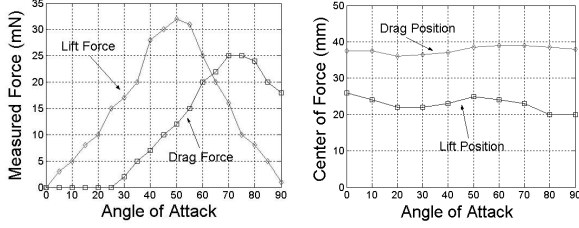


Figure 5: Results from 5X scale experiments

The test procedures for the 1.3X scale spar sensors were similar to that of the 5x scale. However, since the results from the 5X scale experiments showed that the position of the center of force remained roughly constant, sensors were only placed at the base of the wing spar as is seen in figure 4. At the 1.3X scale, the wing went through 90° at 85Hz. This gave the results as shown in figure 6.

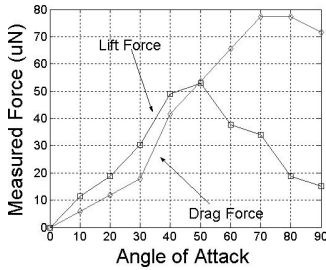


Figure 6: Lift/Drag plots from 1.3X scale

The 1.3X scale results look similar to the 5X scale results, with peaks in the lift and drag forces qualitatively similar to both larger scale results and insect models [4].

4.0 Body Force Measurement

One problem with measuring the flight forces directly on the wing spar is the possible lack of sensitivity at the final scale. One way to alleviate this is to place the sensors away from the thorax, on a more compliant surface measuring the force acting on a beam. Placing the thorax structure on a cantilever to measure the bending moment allows for variable sensitivity. Also, by placing the MFI on a classical dual cantilever system similar to the system described by Abe et al in [1] and Sato et al in [10] and shown in figure 7, the body of the insect is constrained to move in only one line.

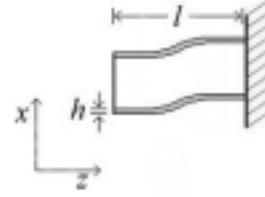


Figure 7: Dual cantilever configuration

Figure 7 shows the deformation of the dual cantilever platform. The load is constrained to move in the x direction and only slightly in the z direction, but since the load always has the same orientation with respect to the horizontal, accurate force readings can be obtained. The second characteristic of such a system is that the stiffness in the z direction is significantly more than in the x direction. The stiffness of the parallel cantilever body force sensor in the x direction is defined by:

$$k_x = \frac{2Eh^3b}{l^3} \quad (4)$$

where E is the Young's Modulus of the material used, h is the thickness of the individual cantilevers, b is the width of the cantilevers, and l is the overall length of the beam. The stiffness in the z direction (without buckling) is expressed as follows:

$$k_z = \frac{Ehb}{l} \quad (5)$$

Thus the ratio of the stiffness in the z direction to the stiffness in the x direction is as follows:

$$\frac{k_z}{k_x} = \frac{l^2}{2h^2} \quad (6)$$

The values of l , h , and b cannot be arbitrarily set, they are constrained by the drive frequency of the MFI wing structure. The parallel cantilever body force sensor (PCBFS) is a resonant system, thus the resonant frequency of the PCBFS must be sufficiently above the drive frequency of the MFI so that the force measuring structure doesn't attenuate the measured MFI forces. Note that the resonance of the PCBFS could be ignored if the desired force readings were not on a stroke-by-stroke basis, that is if the resonant frequency is too low, the PCBFS could measure only an average lift force.

The MFI load mass is approximately 100mg with its actuators and support structure, thus by setting the desired resonant frequency at 500Hz, the remaining parameters can be determined from (4).

Finally, the sensitivity of the structure must be sufficient to measure the small forces generated by the body. The parameters of the PCBFS are set by an optimization

between the resonant frequency and the minimum resolvable force given by the following:

$$F_{\min} = \frac{Eh^3b\varepsilon_{\min}}{12z} \quad (7)$$

Where ε_{\min} is the minimum resolvable strain. The optimization has the two constraints of the 150Hz wing beat frequency, and the weight of the MFI, 1mN which is the minimum force needed to fly, thus F_{\min} will need to be approximately 10 μ N.

It has already been shown that the stiffness in the z direction is large compared to the x direction. This is true also for the y direction. Thus one of the drawbacks of the PCFBS is the difficulty to measure forces in orthogonal directions simultaneously. There are number of ways to obtain two sensing degrees of freedom with the parallel cantilever configuration. One would be to put two identical sensors in series, sensing in orthogonal directions. This however would place too much mass at the end of the first sensor, causing either too low a resonant frequency, or not sufficient sensitivity. Another method is to place the two sensors in parallel, or 'convolve' the two together as shown in figure 8.

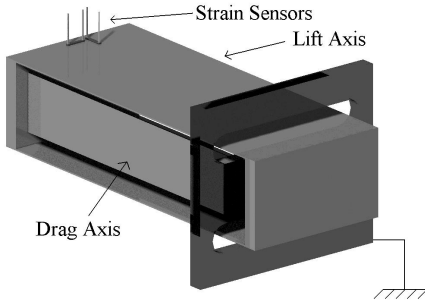


Figure 8: 2DOF PCBFS

Ideally, the two convolved body force sensors would have identical resonant frequencies and sensitivities. This is not possible for the two degree of freedom (DOF) PCBFS if each PCBFS has the same dimensions since adding the second sensing dimension effectively adds a mass in one direction. Using the same dimensions, it is possible to achieve the same sensitivity, however the added mass will result in a lower resonant frequency. Thus it is necessary to alter the dimensions of one of the degrees of freedom. The only difference in design parameters for this case is the added mass of the second sensor. The assumption is made that the torsional stiffness is sufficiently large such that the effective mass on the x-axis is just the second sensor mass added to the load mass. Table 2 shows the parameters used in the construction of the 2DOF PCBFS.

Parameter	Description	Value (est.)	Value (act.)	Units
F_{\min}	Sensitivity	1.00E-05	4.00E-05	N
f_n	Resonant Frequency	5.00E+02	3.25E+02	Hz
E	Modulus (Stainless)	2.00E+02	2.00E+02	GPa
b_x	Cantilever Width - X axis	4.00E-03	4.00E-03	m
b_y	Cantilever Width - Y axis	5.00E-03	5.00E-03	m
h	Cantilever Thickness	7.50E-05	7.50E-05	m
m	Load Mass	1.00E-03	1.00E-03	kg

Table 2: 2DOF PCBFS parameters

4.1 Body Force Sensing Results

At the time of construction of the body force sensor, the thorax for the MFI was too massive to be used as a test subject. Instead a live blowfly (*Calliphora*) was tethered to the force platform using methods similar to Lehman and Dickinson in their work on *Drosophila* as described in [8]. First the sensor was calibrated in both directions by applying incremental known forces and fitting the results to a line. Next, the frequency response was determined by fixing a piezo-electric actuator as a cantilever on the sensor. The actuator cantilever had a mass equivalent to the MFI design parameter of 100mg fixed to its free end. The results are show in figure 9. Note that the stiffness of the actuator was such that with the mass on the free end, its resonant frequency was well below that of the PCBFS, which had a resonant frequency of 325 Hz.

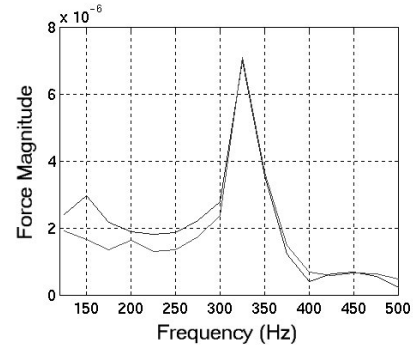


Figure 9: Frequency response of 2DOF PCBFS

Preparation of the animal was in a manner similar to that described by Lehman and Dickinson in [8]. The fly was first anesthetized by cooling to approximately 4° C on a Peltier stage (Teca model LHP-300CP liquid cooled cool plate). It was then tethered at the notum of the thorax with a tungsten rod 0.1mm in diameter. Attachment was made using a UV adhesive (Loctite 352). Before testing, the *Calliphora* was given sufficient time to recover from the effects of cold temperature and UV radiation. The *Calliphora* was fed with sugar water, and readings were made while the insect was active.

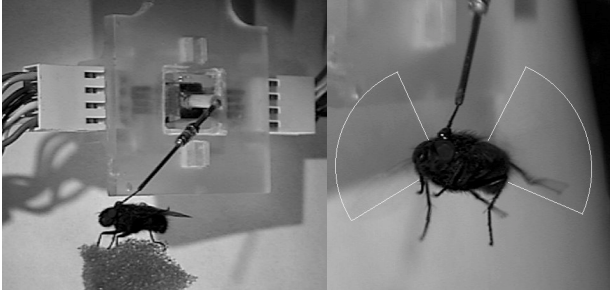


Figure 10: 2DOF body force setup with Calliphora

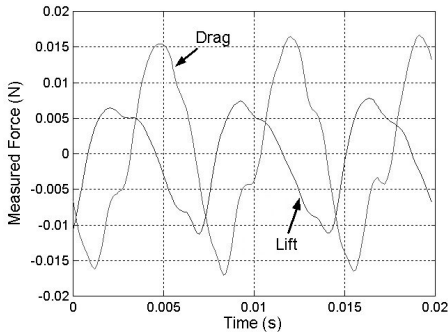


Figure 11: Results from Calliphora body force measurement

The results from the Calliphora experiment showed a number of things. First, this blowfly had a wingbeat frequency of 160Hz on average, and the bandwidth of the PCBFS is sufficiently large to measure this. Second, the Calliphora produced peak forces as high as 12 times its body weight, which is assumed to be mostly the inertial force from its wings, implying a higher Q than in free flight.

5.0 Actuator Force Measurement

Placing strain sensors on the wings or the wing spars has a few drawbacks. First the gages and wires have the potential to add a significant inertial loading. Limited area and delicate surfaces cause the placement of the gages to be both critical and painstaking. Finally, and most significantly, the lead wires from the gages must go through a large stroke angle with the wing causing both high fatigue in the wires and a possibly large parallel stiffness to be introduced. For these reasons, strain sensors were also placed on the MFI thorax. All discussion on actuator-based sensors refers to a 1DOF 1.3X scale fourbar/wing spar structure.

Gage placement directly on the actuator will be contrasted with measurements taken directly on the wing spar. Because of the high transmission ratio of the fourbar, the largest forces in the thorax will develop at the base of the actuator, giving greater sensitivity than

measurements taken directly on the wing spar. However, if the serial stiffness of the fourbar is sufficiently small, or the inertia too large, there will be a phase lag in the measurements at the two points. Also, since the actuator will move the smallest amount of any component in the thorax, the wiring problems are less substantial than placing the gage at any other point. It will be shown that not only does placing the sensors on the actuator produce more accurate results with easier manufacturing, but with actuator sensing, the position of the wing can also be extracted.

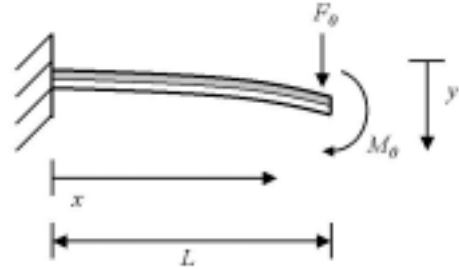


Figure 12: Parameters of the actuator

Consider the simplified drawing of the actuator shown in figure 12. There are two unknown parameters F_0 , the force acting on the slider crank, and the displacement of the proximal end of the slider crank, y . It will be shown that these two can be recovered by measuring the applied voltage V and the strain signal at any point along the actuator. For the quasi-static case, the total moment at any point consists of an internal moment generated by the piezo electric effect, and a moment generated by the force of the slider crank on the tip of the actuator.

$$\epsilon_x \propto M_x = F_0(L-x) + M_0 \quad (8)$$

Thus the bending moment at any point along the actuator can be directly measured. If the internal moment, generated by the piezo is known, along with all the parameters of the actuator, then the force applied to the slider crank is known.

The moment generated by a unimorph piezo-electric actuator is well characterized. By applying an electric field, the piezo-ceramic layer will contract, forming a strain in the elastic layer of the actuator. This strain creates a moment in the actuator, causing it to bend. First, the quasi-static deflection of any point x along the actuator is defined by Smits [14] as follows:

$$y(x) = \frac{3s_s s_p h_s (h_s + h_p) x^2 d_{31} V}{K} \quad (9)$$

where s_s and s_p are the compliance under mechanical stress of the stainless steel layer and piezo layer, respectively, h_s and h_p are the thicknesses of the two layers, d_{31} is the piezo electric constant, V is the applied voltage, and K is defined as follows:

$$K = 4s_p s_s h_s h_p^3 + 4s_p s_s h_s^3 h_p + s_p^2 h_s^4 + s_s^2 h_p^4 + 6s_p s_s h_s^2 h_p^2 \quad (10)$$

Finally, to get the moment, M_0 , generated by the applied voltage note that:

$$\frac{d^2 y(x)}{dx^2} = \frac{M_0}{EI} \quad (11)$$

Thus by integrating:

$$M_0 = \frac{6s_p s_s h_s (h_s + h_p) d_{31} V}{K} \cdot EI \quad (12)$$

Now, from (8), and from measuring the strain and the applied voltage, the force F_0 can be found. The second parameter which is desired is the displacement at the tip. For a free cantilever, this is given by (9). However, the force applied to the tip needs to be taken into consideration. Adding this term into (9) gives the following:

$$y(l) = \frac{M_0 l^2}{2EI} + \frac{F_0 l^3}{3EI} \quad (13)$$

Now each parameter in (13) is known, thus by knowing the strain at any point along the actuator, and the applied voltage, the force and displacement at the free end of the actuator can be solved for. Again, since the first term in (8) is proportional to the distance from the tip to the gage, it is best to place the gage as close to the base as possible. Note also that this is for quasi-static cases, however it is assumed that the drive frequency will be at least an order of magnitude lower than the actuator resonance [16].

Now, at any point in the wing stroke the force applied to the slider crank, and the position of the slider crank is known. From this it is desired to know the torque applied to, and the angle of the wing spar. Under ideal conditions the fourbar will act as an ideal mechanical transformer [13], turning small amplitudes and large forces into large amplitudes and small torques. However, since the system will be operating at resonance, the inertia, damping, and parallel stiffness of the fourbar will contribute to the overall dynamics. If the fourbar parameters are known, then the torque and displacement of the wing spar can be determined. In addition, by assuming negligible dynamics within the differential, the wing rotation angle, stroke angle and torque are known.

For the 1-DOF case, the first step is to determine the torque applied to the wing spar. The torque and displacement of the spar have the following relationship:

$$\tau = J\ddot{\delta} + b\dot{\delta} \quad (14)$$

where J_w and b_w are the inertia and damping of the wing, and τ and δ are the output torque and spar angle for the spar. Taking the Laplace transform of (14), and including all the parameters of the thorax gives the transfer function for the fourbar.

$$\frac{\Delta(s)}{T(s)} = \frac{1}{J' \cdot s^2 + b' \cdot s + k'_p} \quad (15)$$

In (15), J' is the combined inertia of the actuator, fourbar, and wing, b' is the damping of the actuator, fourbar, and wing, and k'_p is the parallel stiffness of the actuator and fourbar. The linear force applied to the slider crank (F), and Y is the displacement of the proximal end of the slider crank. The terms F and Y are related to the output parameters τ and δ by the following:

$$T_w(s) = T(s) - \Delta(s) \left((J_a + J_{4R}) \cdot s^2 + (b_a + b_{4R}) \cdot b \cdot s + k' \right) \quad (16)$$

$$Y = T\delta$$

Here, T is the transmission ratio of the slider crank and fourbar structure and T_w is the wing torque. Now the output angle and torque can be solved for by simple filtering.

5.1 Actuator Sensor Results

A one DOF wing thorax and wing structure were made and strain sensors were placed at the base of the actuators. Table 3 shows the parameters of the system, and figure 13 shows the force and position plots for the wing and actuator over a few periods.

Parameter	Description	Value	Units
K_a	Actuator Stiffness	3.1E+02	N/m
b_a	Actuator Damping	1.7E-03	Ns/m
J_a	Actuator Inertia	7.4E-05	kg
K_{4R}	Fourbar Parallel Stiffness	6.1E-04	Nm/rad
b_{4R}	Fourbar Damping	8.0E-09	Nms/rad
J_{4R}	Fourbar Inertia	1.2E-10	kgm ²
b_w	Wing Damping	3.2E-08	Nms/rad
J_w	Wing Inertia	2.0E-10	kgm ²
T	Fourbar Transmission Ratio	5.0E+03	rad/m
Q	Q of the Thorax	3	
ω	Resonant Frequency	471	rad/s

Table 3: 1 DOF MFI wing transmission parameters

Assuming that the forces on the wing act on the center of area [13], the combined aerodynamic and inertial force acting on the wing can be extracted from the wing torque. Figure 13 show a wing force of approximately 150 μ N peak-peak, thus with a Q of 3, and from (3), there is 50 μ N peak-peak aerodynamic force. Since this is in the drag plane, this can be compared with the results from section 3 which showed a 70 μ N peak-peak force using the spar sensor under similar conditions.

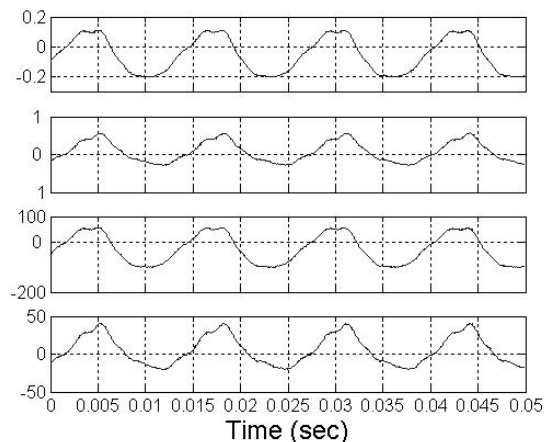


Figure 13: From top, plots of actuator force (N), actuator displacement (mm), wing force (μN), and wing angle (degree)

6.0 Discussion

Currently, in parallel with the development of the MFI flight force sensors is the development of the 2DOF resonant structure as described in [13]. In the near term, the thorax and wing structure will be reduced in weight and size to be fit onto the 2DOF PCBFS. Also, the techniques described in section 3.3 are being applied to the construction processes of the MFI thorax.

Acknowledgments

The authors would like to thank Joe Yan for his help with the fly cooling and handling, The Michael Dickinson lab for the Calliphora, and Srinath Avadhanula for helpful discussions on thorax dynamics. This work was funded by NSF KDI ECS 9873474, ONR MURI N00014-98-1-0671, and DARPA.

References

- [1] K. Abe, T. Miwa, and M. Uchiyama. Development of a 3-axis planar force/torque sensor for very small force/torque measurement. *Trans Jpn Soc Mech Eng*, Vol 42, No. 2, pages 376-382, 1999.
- [2] A. Bicchi, A. Caiti, and D. Prattichizzo. Optimal design of a multi-axis force/torque sensor. *IEEE Intl Conf on Decision and Control*, pages 2981-2986, Phoenix, AZ, Dec 1999.
- [3] J.H. Cocatre-Zilgien and F. Delcomyn. Modeling stress and strain in an insect leg for simulation of campaniform sensilla responses to external forces. *Biological Cybernetics*, Vol. 81, No. 2, pages 149-60, Springer-Verlag, Aug. 1999.
- [4] M.H. Dickinson, F-O. Lehmann, and S.P Sane. Wing rotation and the basis of insect flight. *Science*, 284:1954-1960, June 1999.
- [5] S Fahlbusch and S. Fatikow. Force sensing in microrobotic systems – an overview. *IEEE Intl Conf on Electronics, Circuits and Systems*, pages 259-262, Lisbon, Portugal, Sept 1988.
- [6] R.S. Fearing, K.H. Chiang, M.H. Dickinson, D.L. Pick, M. Sitti, and J. Yan. Wing transmission for a micromechanical flying insect. *IEEE Intl Conf on Robotics and Automation*, pages 1509-1516, San Francisco, CA, April 2000.
- [7] M.L. Jakobsen, T.P. Dewhurst, and C.A. Greated. Particle image velocimetry for predictions of acceleration fields and force within fluid flows. *Measurement Science & Technology*. Vol.8, No.12, p.1502-16, IOP Publishing, Dec. 1997.
- [8] F-O. Lehmann and M.H. Dickinson. The changes in power requirements and muscle efficiency during elevated force production in the fruitfly *Drosophila Melanogaster*. *Journal of Experimental Biology*, Vol. 200, No. 7, pages 1133-1143, April 1997.
- [9] G. Nalbach. The halteres of the blowfly *Calliphora*. *Journal of Comparative Physiology A-Sensory Neural and Behavioral Physiology*, No. 173, pages 293-300, 1993.
- [10] H. Sato, T. Fukuda, F. Arai, H. Iwata, and K. Itoigawa. Analysis of parallel beam gyroscope. *IEEE Intl Conf on Robotics and Automation*, pages 1632-1637, Detroit, Michigan, May 1999.
- [11] L. Schenato, X. Deng, and S. Sastry. Flight control system for a micromechanical flying insect: architecture and implementation. *IEEE Intl Conf on Robotics and Automation*, Seoul, Korea, May 2001.
- [12] E. Shimada, J.A. Thompson, J. Yan, R.J. Wood, and R.S. Fearing. Prototyping millirobots using dextrous microassembly and folding. *Symp on Microrobotics ASME Intl Mech Eng Cong and Expo*, Orlando, FL, Nov 5-10, 2000.
- [13] J. Yan, R.J. Wood, S. Avadhanula, M. Sitti, and R.S. Fearing. Towards flapping wing control for a micromechanical flying insect. *IEEE Intl Conf on Robotics and Automation*, Seoul, Korea, May 2001.
- [14] J. Smits and W. Choi. The constituent equations of piezoelectric heterogeneous bimorphs. *IEEE Tran. On Ultrasonics, Ferroelectrics, and Freq. Control*, vol. 38, pages 256-270, May 1991.
- [15] M. Weinberg. Working equations for piezoelectric actuators and sensors. *Journal of Microelectromechanical Systems*, vol. 8, pages 529-533, Dec. 1999.
- [16] M. Sitti, D. Campolo, J. Yan, R. S. Fearing, T. Su, D. Taylor. Development of PZT and PZN-PT based unimorph actuators for micromechanical flapping structures. *IEEE Intl Conf on Robotics and Automation*, Seoul, Korea, May 2001.